

# Soft Matter

Accepted Manuscript



This is an *Accepted Manuscript*, which has been through the Royal Society of Chemistry peer review process and has been accepted for publication.

*Accepted Manuscripts* are published online shortly after acceptance, before technical editing, formatting and proof reading. Using this free service, authors can make their results available to the community, in citable form, before we publish the edited article. We will replace this *Accepted Manuscript* with the edited and formatted *Advance Article* as soon as it is available.

You can find more information about *Accepted Manuscripts* in the [Information for Authors](#).

Please note that technical editing may introduce minor changes to the text and/or graphics, which may alter content. The journal's standard [Terms & Conditions](#) and the [Ethical guidelines](#) still apply. In no event shall the Royal Society of Chemistry be held responsible for any errors or omissions in this *Accepted Manuscript* or any consequences arising from the use of any information it contains.

# Spontaneous motility of passive emulsion droplets in polar active gels

G. de Magistris<sup>a</sup>, A. Tiribocchi<sup>a</sup>, C. A. Whitfield<sup>b</sup>, R. J. Hawkins<sup>b</sup>, M. E. Cates<sup>a</sup>, D. Marenduzzo<sup>\*a</sup>

Received Xth XXXXXXXXXXXX 20XX, Accepted Xth XXXXXXXXXXXX 20XX

First published on the web Xth XXXXXXXXXXXX 200X

DOI: 10.1039/b000000x

We study by computer simulations the dynamics of a droplet of passive, isotropic fluid, embedded in a polar active gel. The latter represents a fluid of active force dipoles, which exert either contractile or extensile stresses on their surroundings, modelling for instance a suspension of cytoskeletal filaments and molecular motors. When the polarisation of the active gel is anchored normal to the droplet at its surface, the nematic elasticity of the active gel drives the formation of a hedgehog defect; this defect then drives an active flow which propels the droplet forward. In an extensile gel, motility can occur even with tangential anchoring, which is compatible with a defect-free polarisation pattern. In this case, upon increasing activity the droplet first rotates uniformly, and then undergoes a discontinuous nonequilibrium transition into a translationally motile state, powered by bending deformations in the surrounding active medium.

## 1 Introduction

Active matter is an exciting area of physics which has gathered a lot of interest within the last few years. Active systems are those in which constituents take up energy from the environment and exert non-thermal (“active”) forces on their surroundings – generally to propel themselves. While less studied than self-propelled hard-sphere particles (see Refs.<sup>1–5</sup> for some examples out of many), the case of self-motile fluid droplets has attracted considerable interest<sup>6–13</sup>. Such droplets, which may provide a minimal model of a moving cell fragment, show a diversity of propulsion mechanisms that involve a coupling between motion and internal deformations. Our goal here is to study a third class of system in which motility can arise spontaneously. We consider a droplet of passive, isotropic Newtonian fluid embedded in an active polar liquid crystal (or active gel), representing a fluid containing force dipoles with long-range orientational order. These isotropic droplets are set into motion by their creation of a non-trivial force distribution in their immediate surroundings. This interaction therefore harnesses the activity of the surrounding medium, causing the passive droplet to move with finite velocity under conditions we describe below.

Active gels are by now paradigms for the theory of active matter physics<sup>1,2</sup>. Their hydrodynamics has received a lot of attention<sup>14–20</sup>, because it entails a number of surprising purely non-equilibrium effects, such as the creation of spontaneous flow<sup>15</sup>. Active gels also exhibit an exotic response to external flows and highly nontrivial microrheological properties<sup>21–25</sup>. From an experimental point of view, the best known realisa-

tions of active gels are actomyosin solutions<sup>26,27</sup> and bacterial suspensions<sup>28,29</sup>. In the former, the dipolar forces (exerted by the myosin molecular motors) are contractile, while the latter are an examples of extensile active fluids. In both cases, one should keep in mind that while standard active gel theory is a very useful starting point, it probably provides at best a rather coarse approximation of such systems. For instance, in actomyosin systems, molecular motors often tend to form large clusters<sup>26</sup> which when present would lead to effects not included in theories for one-component active fluids. Meanwhile bacterial suspensions of high enough concentration to observe local liquid crystalline order are relatively uncommon (although they do exist<sup>29</sup>). Very recently, Sanchez et al.<sup>30,31</sup> have however proposed an intriguing minimal *in vitro* model where microtubule bundles, formed by depletion interaction due to polyethylene glycol, interact with kinesin motors; this system may provide a simpler laboratory realisation of an active extensile fluid, albeit nematic and not polar\*.

We will show below that the inverted droplet geometry is of high theoretical interest, because it leads to novel motility scenarios. As we shall see, the isotropic droplets in our system are moved around by the active forces in the surrounding fluid, through two distinct mechanisms involving elastic deformations in the polarisation field, outside the droplet in the active gel phase. In one case, motion is triggered by a localised flow close to a topological defect which arises near the droplet surface due to the anchoring of the director field at that surface. In the second case, motion is powered by spontaneous flow in the bulk, which is accompanied by a bulk elastic dis-

\*The fact that the active gel in Refs.<sup>30,31</sup> is nematic allows for topological defects of half-integer charge, and this may lead to significant differences for our system. This may be of relevance in the case where there is normal anchoring at the droplet surface, when a hyperbolic hedgehog defect forms (see e.g. Fig. 1). When defects are not present, on the other hand, we expect the polar and nematic systems to behave similarly.

<sup>a</sup> SUPA, School of Physics and Astronomy, University of Edinburgh, Mayfield Road, Edinburgh EH9 3JZ, UK

<sup>b</sup> Department of Physics and Astronomy, University of Sheffield, Sheffield S3 7RH, UK

tortion in the active phase. Besides characterising the physics of these motile droplet configurations in our simulations, we discuss how to test our predictions in the laboratory.

Our work is structured as follows. In Section 2 we introduce the methods we employ to solve the hydrodynamic equations of motion for our two dimensional model system. In Section 3 we report our results, starting from the baseline case of an emulsion droplet inside a passive liquid crystal, before moving on to the various active scenarios. In Section 4, we conclude by discussing our results in view of current experiments on active droplets and active matter more generally.

## 2 Simulation model and methods

The physics of an isotropic droplet dispersed in an active polar liquid crystal can be described in terms of a set of coarse-grained variables  $\phi(\mathbf{r}, t)$ ,  $\mathbf{P}(\mathbf{r}, t)$ ,  $\rho(\mathbf{r}, t)$ ,  $\mathbf{v}(\mathbf{r}, t)$ , which are, respectively: an order parameter describing concentration variations; the polarisation associated with the liquid crystal phase<sup>†</sup>; the mass density (in our case constant to a good approximation); and the average velocity field, which governs both the solvent and the solute flow. Working in two dimensions, we construct our passive isotropic droplet by initializing a circular region in which the concentration and the polarisation of the active material are zero in the interior ( $\phi = 0$ ,  $\mathbf{P} = 0$ ). These quantities are finite outside ( $\phi > 0$ ,  $\mathbf{P} \neq 0$ ) and initially uniform. The equilibrium properties of a purely passive system are encoded in a free energy, whose full expression is<sup>11,32,33</sup>

$$F[\phi, \mathbf{P}] = \int d^3r \left\{ \frac{a}{4\phi_{cr}^4} \phi^2 (\phi - \phi_0)^2 + \frac{k}{2} |\nabla\phi|^2 - \frac{\alpha (\phi - \phi_{cr})}{2 \phi_{cr}} |\mathbf{P}|^2 + \frac{\alpha}{4} |\mathbf{P}|^4 + \frac{\kappa}{2} (\nabla\mathbf{P})^2 + \beta_1 \mathbf{P} \cdot \nabla\phi + \beta_2 (\mathbf{P} \cdot \nabla\phi)^2 \right\}. \quad (1)$$

This free energy combines two principal contributions: the first two terms, which stem from a typical binary fluid formalism, and the remaining part which is borrowed from liquid crystal theory. In particular the first term of Eq.(1) is a double well potential allowing bulk phase separation into a dense (exterior) and dilute (interior) phases in the droplet geometry. The second term creates an interfacial tension between these phases whose strength depends on  $k$ . The remaining terms in the free energy (the ones taken from liquid crystals) are made up of three different contributions. The first one, comprising of all the term multiplied by the factor  $\alpha$ , is the bulk free energy associated with the polar phase, which contains terms in the polarisation  $\mathbf{P}$  up to the fourth order. In the quadratic

contribution, which also depends on  $\phi$ ,  $\phi_{cr}$  is the critical concentration for the transition from isotropic ( $|\mathbf{P}| = 0$ ) to polar ( $|\mathbf{P}| > 0$ ) states. The value of  $\phi_{cr}$  is chosen such that activity only arises in the region exterior to the droplet, once equilibrium values of the concentration  $\phi_{eq}$  and polarisation  $\mathbf{P}_{eq}$  are obtained by minimizing the free energy. The term in  $(\nabla\mathbf{P})^2$  creates an elastic penalty for local distortions of the polar order, within the (standard) ‘‘one elastic constant’’ approximation<sup>34</sup>, with  $\kappa$  the resulting single elastic constant. Finally the last two terms take into account the anchoring of  $\mathbf{P}$  on the surface of the droplet. The first of these, involving  $\beta_1$ , models homeotropic (normal) anchoring: at the surface of the droplet,  $\mathbf{P}$  will point inwards if  $\beta_1 > 0$  and outwards if  $\beta_1 < 0$ . A second term, quadratic in  $\mathbf{P}$  and in the gradient of  $\phi$ , needs to be included when tangential (planar) anchoring is required. Such anchoring arises when  $\beta_1 = 0$  and  $\beta_2$  is positive. The magnitude of  $\beta_1$  or  $\beta_2$  controls the anchoring strength; we assume strong alignment throughout our simulations.

The dynamical equations describing the evolution of the aforementioned coarse-grained variables are<sup>11</sup>

$$\nabla \cdot \mathbf{v} = 0, \quad (2)$$

$$\rho \left( \frac{\partial}{\partial t} + \mathbf{v} \cdot \nabla \right) \mathbf{v} = -\nabla P + \nabla \cdot (\underline{\underline{\sigma}}^{\text{act}} + \underline{\underline{\sigma}}^{\text{pass}}), \quad (3)$$

$$\frac{\partial \phi}{\partial t} + \nabla \cdot (\phi \mathbf{v}) = \nabla \cdot \left( M \nabla \frac{\delta F}{\delta \phi} \right), \quad (4)$$

$$\frac{\partial \mathbf{P}}{\partial t} + (\mathbf{v} \cdot \nabla) \mathbf{P} = -\underline{\underline{\Omega}} \cdot \mathbf{P} + \underline{\underline{\xi}} D \cdot \mathbf{P} - \frac{1}{\Gamma} \frac{\delta F}{\delta \mathbf{P}}. \quad (5)$$

The first two equations are, respectively, the continuity and the Navier-Stokes equations for an incompressible fluid. The right hand side of Eq.(3) represents the force density acting on the fluid and is made up of two contributions, the first of which is the gradient of an isotropic pressure field  $P$  and the second is the gradient of the total stress tensor, which is in turn the sum of an active and a passive term. The active part is given by

$$\underline{\underline{\sigma}}_{\alpha\beta}^{\text{act}} = -\zeta \phi P_{\alpha} P_{\beta}, \quad (6)$$

where, here and in what follows, Greek indices denote Cartesian coordinates, while  $\zeta$  is the activity parameter which can be negative or positive, for contractile or extensile particles, respectively. This form of active stress can be directly derived by summing the contributions from each force dipole and coarse graining; the magnitude of  $\zeta$  is then fixed by the density and strength of the force dipoles<sup>33</sup>. These forces are generated by using up energy, e.g. coming from ATP hydrolysis<sup>14</sup>.

The passive contribution to the stress tensor is the sum of

<sup>†</sup> The polarisation  $\mathbf{P}$  represents the mesoscopic average orientation of the polar particles (in our case these can be single actin fibre, bundles of actin filaments or microtubules).

three different terms<sup>11</sup>

$$\sigma_{\alpha\beta}^{visc} = \eta(\partial_\alpha v_\beta + \partial_\beta v_\alpha), \quad (7)$$

$$\sigma_{\alpha\beta}^{elas} = \frac{1}{2}(P_\alpha h_\beta - P_\beta h_\alpha) - \frac{\xi}{2}(P_\alpha h_\beta + P_\beta h_\alpha) - \kappa \partial_\alpha P_\gamma \partial_\beta P_\gamma, \quad (8)$$

$$\sigma_{\alpha\beta}^{inter} = \left( f - \phi \frac{\delta F}{\delta \phi} \right) \delta_{\alpha\beta} - \frac{\partial f}{\partial (\partial_\beta \phi)} \partial_\alpha \phi. \quad (9)$$

The first of these term is the viscous stress, with  $\eta$  the shear viscosity. The second is the stress due to elastic distortions in the liquid crystal, with  $\mathbf{h} = \delta F / \delta \mathbf{P}$  the molecular field. The constant  $\xi$  is related to the aspect ratio of active particles<sup>14</sup>: it is positive for rod-like particles and negative for disc-like ones. Here we set it positive as in previous works<sup>11,32</sup>. This parameter also controls whether particles are flow-tumbling or flow-aligning under imposed shear. In the flow-tumbling case, observed for small enough  $\xi$ , particles reorient chaotically (even without activity), whereas in the flow-aligning case, which we choose for simplicity throughout this paper, they align at a fixed angle to the flow direction, called the Leslie angle. The last contribution to the stress tensor is an interfacial term caused by concentration gradients at the perimeter of the droplet.

The time evolution of the concentration field  $\phi(\mathbf{r}, t)$  is described by Eq.(4). This is a convection-diffusion equation;  $M$  is a thermodynamic mobility parameter and  $\delta F / \delta \phi$  is the chemical potential. The dynamics of the vector polarisation field  $\mathbf{P}(\mathbf{r}, t)$  is described by Eq.(5), which is a convection-relaxation equation. On the right hand side  $\underline{D}$  and  $\underline{\Omega}$  represent the symmetric and the antisymmetric part of the the velocity gradient tensor  $\nabla \mathbf{v}$ , and  $\Gamma$  is a parameter called the rotational viscosity.

Eqs.(2-5) are solved numerically by using a hybrid lattice Boltzmann method previously tested in similar systems, such as liquid crystals<sup>35</sup> or active matter<sup>11,32,36</sup>. By using lattice Boltzmann, this method trades off small departures from incompressibility for much faster numerics in what is then a fully local description of momentum transport. Meanwhile  $\phi$  and  $\mathbf{P}$  are evolved using finite difference methods which are more efficient for these quantities. Each time step, local information on the various fields is exchanged between the two parts of the algorithm.

Where not explicitly stated, most of the runs were performed on rectangular periodic lattices using the following parameter values:  $a = 0.04$ ,  $k = 0.06$ ,  $\Gamma = 1$ ,  $\phi_0 = 2$ ,  $\phi_{cr} = 1$ ,  $\alpha = 0.1$ ,  $\eta = 1$ . These are quoted in simulation units; for a mapping to corresponding values in physical units, see Appendix 1 and the Figure captions. Additional parameters (e.g. describing anchoring) are given in captions to the relevant Figures. Our simulations are two dimensional. For all the reported results the geometry of the 2D simulation box is rectangular, with a longer size along the direction along which the

droplet was found to move: this minimises effects due to interactions with the periodic images of the droplets along the main flow direction.

The polarisation field is always set to zero initially inside the droplet and different from zero outside, where there is the liquid crystal. Furthermore, the concentration field is initially zero inside the droplet, and equal to  $\phi_0$  outside. We note that this initial condition leads to a final droplet size, after equilibration, that depends on the anchoring condition. This does not contradict the fact that our algorithm conserves the order parameter  $\phi$ , because for a droplet geometry in a finite container, the values of  $\phi$  in the two phases deviate in equilibrium from those at the double-well minima of  $F$  (here  $\phi = 0, 2$ ).

This effect is related to interfacial energetics, and indeed is familiar for a simple fluid where the offset it is set by the Laplace pressure. For a droplet in a liquid crystal it turns out to be more pronounced for the normal anchoring case. We interpret this as due to a stronger contribution of the elastic deformations close to the droplet surface in the case of normal anchoring, causing a decrease in the value of  $\phi$  in the polar phase, and hence an increase in droplet size. This effect, which could be countered by increasing the value of  $a$  in Eq. 1, is not relevant when addressing the role of activity in droplet motion, which is the subject of this paper.

### 3 Results

We now present our results. We first recap the physics of a passive droplet in a polar passive liquid crystal, which is a useful background, because it is the system our active mixture reduces to for  $\zeta = 0$ . We then study the active case, first where the polarisation is normal to the droplet at its surface, and then where it is instead tangential.

#### 3.1 Equilibrium states of an isotropic droplet in a passive polar liquid crystal

In the passive case, it is well known that if the polarisation field is anchored normally to the surface of a droplet (or a solid particle), then, if the anchoring is strong, a defect of topological charge  $-1$ , called a hyperbolic hedgehog, forms<sup>37-39</sup>. We note here that if our liquid crystal was apolar, rather than polar, the droplet might instead have been surrounded by a Saturn ring, a disclination loop of defects of half-integer charge: such a defect is not, however, possible with a polar vector field, such as our  $\mathbf{P}$ . The creation of a defect of integer topological charge ( $-1$ ) near the droplet is a topological requirement here, since the polarisation field far away from the droplet is defect free, and the droplet itself with the normal anchoring at the surface is equivalent to a hedgehog defect of topological charge  $+1$ .

Fig. 1b, which shows the equilibrium states of a single isotropic droplet embedded in a passive polar liquid crystal host, with normal anchoring of  $\mathbf{P}$  at its surface, confirms this expectation. The defect is also responsible for the changes in the direction of  $\mathbf{P}$  (initially set along  $x$ ) as reported in Fig. 1c. The two elongated bright patches partially surrounding the droplet identify regions of strong splay-bend distortion where  $\mathbf{P}$  is almost fully along the  $y$ -direction, whereas the dark regions far from the droplet indicate areas where the polarisation is almost completely along  $x$ . A similar structure was originally discussed for nematic liquid crystals in the seminal paper of Lubensky *et al.*<sup>40</sup>.

Changing the anchoring of  $\mathbf{P}$  at the droplet surface from normal to tangential changes the final state considerably. Fig. 2 shows the equilibrium structure obtained with tangential anchoring. The polarisation profile is less distorted now away from the droplet, and the resulting pattern has a quadrupolar, rather than dipolar, symmetry, with moderate splay-bend deformations surrounding the droplet (these are localised around the four symmetric bright regions in Fig. 2c). We note that the structure in Fig. 2c avoids topological defects in the bulk of the liquid crystal by effectively breaking the anchoring where the polarisation field touches the droplet along the  $x$  direction. These points at which the anchoring is broken would lead, in 3D, to boojum-like surface defects, like those observed experimentally by Poulin *et al.* in<sup>41,42</sup>, where water droplets of 1 to 5  $\mu\text{m}$  in diameter were dispersed within a nematic liquid crystal. (In that work, a polymer solution was used to induce strong planar and degenerate anchoring of the director field at the droplet surface, while a surfactant was added to stabilise the droplets.)

### 3.2 Isotropic emulsion droplet in an active polar gel

We now turn to the results obtained when the droplet is embedded into an active, rather than passive, polar fluid. In all cases, the states shown in Fig. 1 and 2 were taken as initial conditions for the runs with activity switched on. The system we study might be realised in experiment by dispersing a (surfactant stabilised) droplet of a Newtonian fluid into a contractile actomyosin gel<sup>26,27</sup>, or perhaps into a mixture of extensile microtubule bundles and kinesin motors. A controlled experiment on either system might well be challenging in practice; nevertheless, it might uncover significant new physics, as we discuss below.

#### 3.2.1 Homeotropic anchoring: contractile gel

We first consider the case in which  $\mathbf{P}$  is homeotropically anchored normal to the droplet's surface. Fig. 3 shows a plot of the steady state drift velocity of a contractile polar fluid as a function of  $\zeta$ . Our numerical simulations show that for

any  $\zeta \neq 0$  the droplet is set in motion by the asymmetric polarisation pattern arising from the presence of the hyperbolic hedgehog at its side. This polarisation pattern sets up an active flow powering the droplet's motion (Suppl. Movie 1). An analysis of the droplet centre of mass velocity shows that for  $|\zeta| \leq 0.00015$  the speed increases linearly with the magnitude of the contractile activity. Dimensional analysis further suggests  $v_{\text{drift}} \sim |\zeta|R/\eta$ , however a full validation of this scaling is difficult in our simulation, as increasing  $R$  would require an increase in system size to avoid finite size effects, and this is known to affect the magnitude of bulk active flow (see e.g.<sup>18,25</sup>). For  $|\zeta| > 0.00015$  there is a deviation from the linear regime, and for sufficiently negative activity the droplet motion becomes apparently chaotic (Suppl. Movie 2).

In Fig. 4 we show the steady states of both the polarisation profile and the corresponding velocity field, for  $\zeta = -0.0001$ , which is within the linear velocity regime. The droplet moves parallel to the positive  $x$ -direction, with the defect at its rear. The droplet preserves its circular shape, and the hyperbolic hedgehog follows it along during the motion. The flow field around the propelled droplet is dipolar (i.e. is a stresslet far from the droplet), and features vortices, which arise due to the active force distribution in the bulk of the contractile gel. There are forces pushing the droplet to the right due to the polarisation splay which are localised at the right and left boundary; these are balanced by opposing forces to the left, again driven by splay, and localised in the bulk of the active gel, where this deformation is largest.

Our droplet becomes motile because of its effect on the bulk polarisation field. In that sense, although it is motile, it is not self-propelled. However, the dipolar (stresslet) fluid flow is indistinguishable from that which would be expected for a self-propelled object which exerts a force distribution around its surface, mirroring that exerted here by the contractile gel. As a result, the exterior flow field strongly resembles that observed in the "direct" active emulsion case, where active gel droplets self-propel when embedded in an isotropic fluid<sup>11</sup>. An important difference is that in the current case there is no activity threshold below which the droplet is static; this is because the anchoring breaks the symmetry in the polarisation pattern even in the passive limit, due to the creation of the hyperbolic hedgehog, and the consequent dipolar nature of the  $\mathbf{P}$  field.

Intriguingly, this highly non-trivial velocity field leaves little sign on the polarisation, which is almost unaffected by the flow. In other words elastic interactions (due to  $\kappa$  and  $\beta_{1,2}$ ) dominate over flow induced reorientation in this regime. Indeed the Ericksen number which measures the ratio between viscous and elastic effects,  $\text{Er} = \Gamma v R / \kappa$ , where  $\Gamma$  is the rotational viscosity of the active gel, and  $v$  is the droplet speed, is still small in our simulations ( $\text{Er} \sim 0.2$  in Fig. 4).

To check that the presence of the images due to the pe-

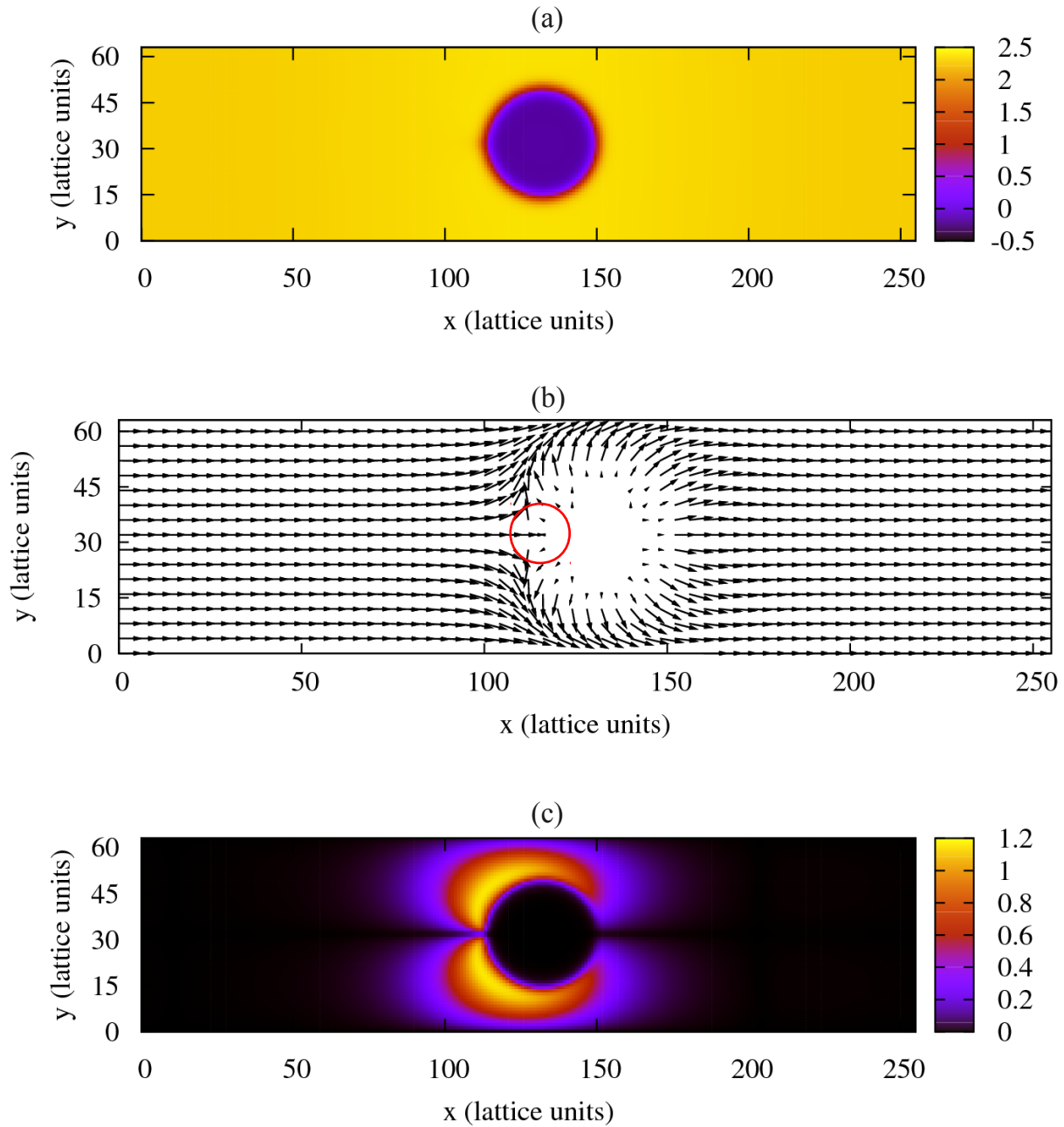


**Fig. 1** a) Equilibrated concentration field of an isotropic droplet (dark/purple) in a passive polar liquid crystal (bright/yellow). b) Polarisation field outside the droplet. Strong homeotropic (normal) anchoring is set on its surface; a defect of topological charge  $-1$  is visible on the left. c) Density plot of the absolute value of the  $y$ -component of  $\mathbf{P}$ . Two bright (yellow) stripes, close to the droplet's surface, identify regions where its value is around 1. We initialised the system with a circular droplet, and with the bulk polarisation in the liquid crystal along the  $x$ -direction,  $\mathbf{P} = [1, 0]$ , on a lattice of dimensions  $L_x = 256$ ,  $L_y = 64$ . The elastic constant is  $\kappa = 0.01$ . In equilibrium, the droplet attains a radius of  $R \sim 17$ . To ensure strong normal anchoring of  $\mathbf{P}$  at the droplet surface, we chose  $\beta_1 = -0.01$  and  $\beta_2 = 0$  in Eq. 1.

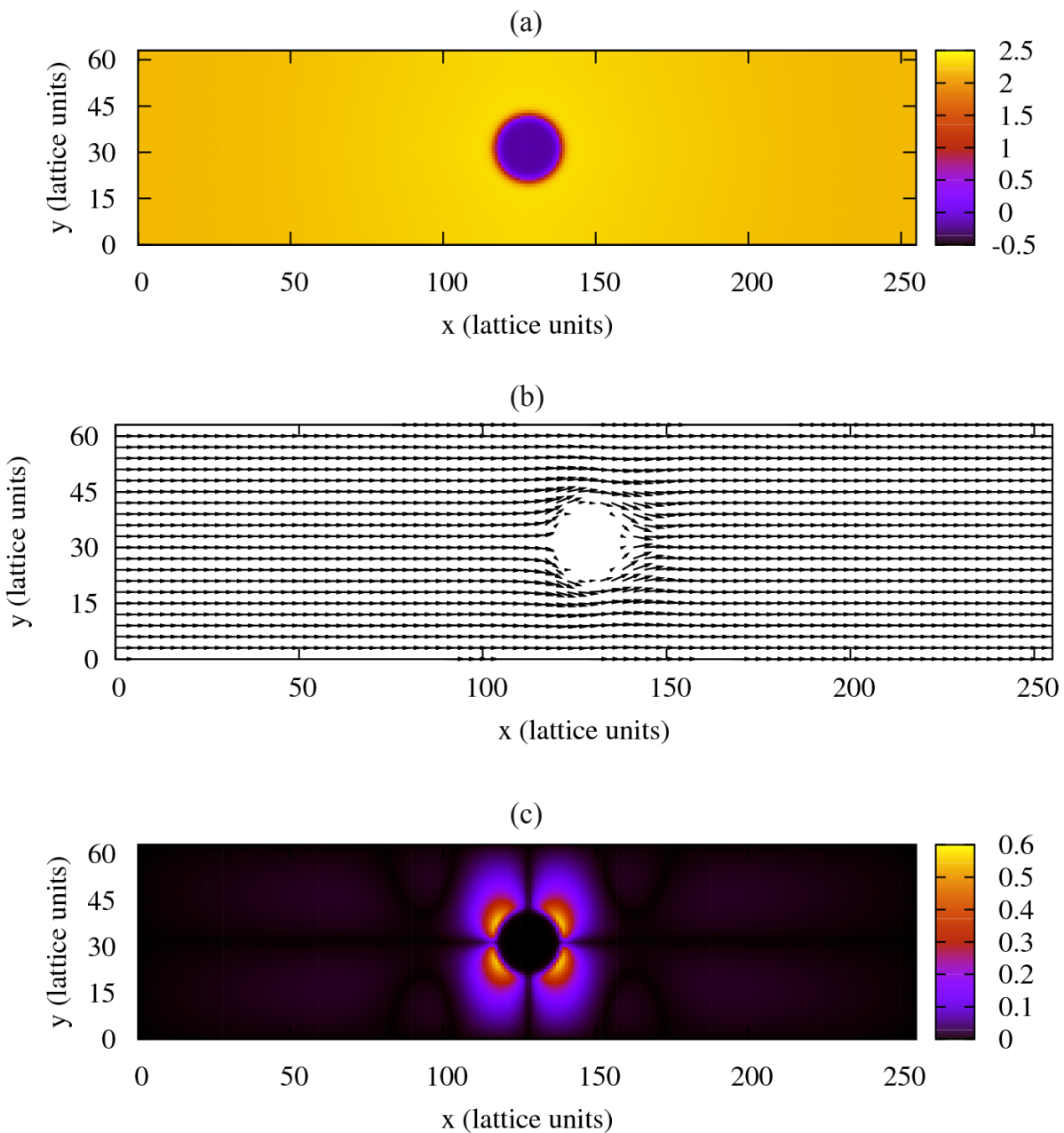


**Fig. 2** a) Equilibrium density field of an isotropic droplet (dark/purple) in a passive polar liquid crystal (bright/yellow). b) Polarisation field outside the droplet. Strong tangential anchoring is set on its surface. c) Density plot of the absolute value of the  $y$ -component of  $\mathbf{P}$ . Four almost symmetric bright spots, close to the droplet's surface, identify regions where its value is around 0.6. To set up the simulation, we initialized the droplet as in Fig. 1, with the bulk polarisation in the liquid crystal initially along  $x$ . To ensure tangential anchoring, we set  $\beta_1 = 0$  and  $\beta_2 = 0.01$ . The elastic constant is  $\kappa = 0.01$ . In equilibrium, the droplet attains a radius of  $R \sim 11$  (in simulation units).

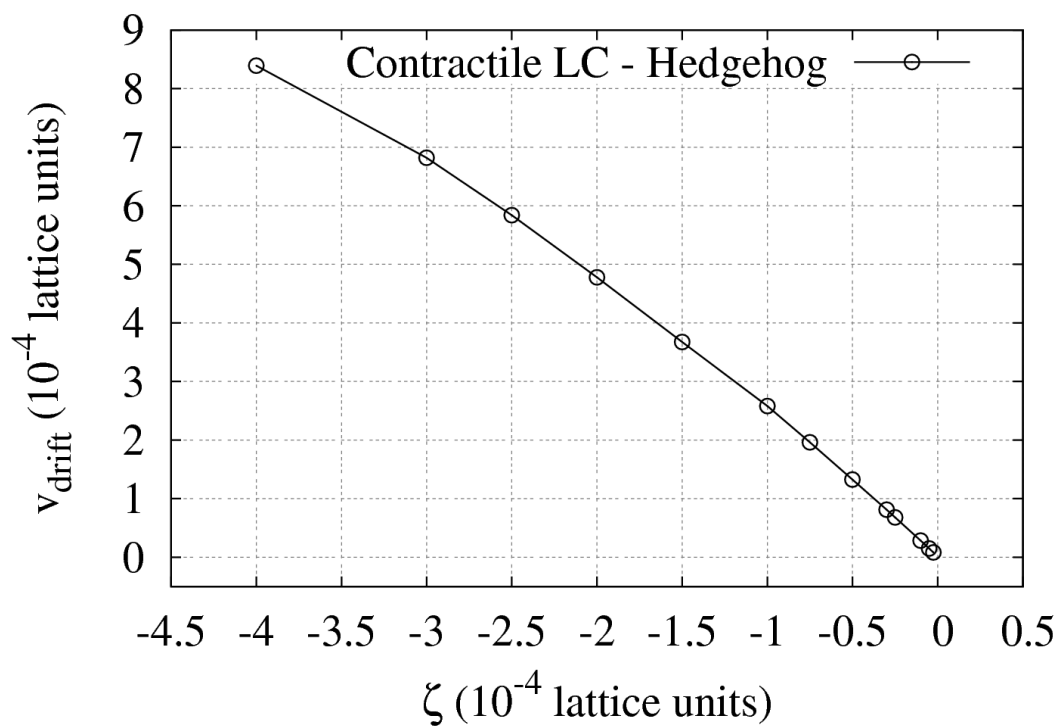


**Fig. 3** Steady state drift velocity as a function of the activity for a contractile system with homeotropic anchoring on the droplet's surface. For  $|\zeta| < 0.00015$  (corresponding to a contractile active stress of 15 Pa, see mapping in Appendix 1) the dependence is linear, whereas for more strongly negative values there is a deviation. The elastic constant is  $\kappa = 0.02$  (2 pN).

riodic boundary conditions do not lead to artifacts, we also performed simulations with a larger lattice, and found similar results (Suppl. Fig. 1).

It is also possible to derive analytical expressions for the equilibrium polarisation, in the zero activity limit, and for the active force distribution in the small activity limit, which help understand our numerical results for this homeotropic anchoring case. In 2D, and in polar coordinates ( $r$  and  $\theta$ , with the centre of the droplet as the origin) the polarisation along the radial and angular directions can be found as in Ref.<sup>40</sup>, and are explicitly given by  $p_r = \cos(\alpha)$  and  $p_\theta = \sin(\alpha)$  respectively, where:

$$\alpha = \theta - \tan^{-1} \left( \frac{r \sin(\theta)}{r \cos(\theta) + Rc_0} \right) - \tan^{-1} \left( \frac{r \sin(\theta)}{r \cos(\theta) + R/c_0} \right) \quad (10)$$

where  $R$  is the droplet radius and  $Rc_0$  is the distance of the hedgehog defect from the centre of the droplet. The resulting profile makes sense only for  $r \geq R$  and compares well with the numerics (compare Suppl. Fig. 2 and Fig. 1).

Simulations and intuition suggest that Eq. 10 still describes the system well for small values of  $\zeta$ , and in this limit the stress will be dominated by the active contribution as the thermodynamic one will be zero. The active force density can then be written as  $f_\alpha^{\text{act}} = \partial_\beta \sigma_{\alpha\beta}^{\text{act}}$  (or in vector notation  $\mathbf{f}^{\text{act}} = \nabla \cdot \underline{\underline{\sigma}}^{\text{act}}$ ); its  $x$  contribution is plotted in Suppl. Fig. 3. After some algebra, we can calculate the net force density on the droplet boundary in the  $x$ -direction as an integral over  $\theta$ , as follows:

$$\frac{1}{2\pi} \int_{-\pi}^{\pi} (\nabla \cdot \underline{\underline{\sigma}}^{\text{act}}) \cdot \hat{\mathbf{x}} d\theta = -\frac{\zeta \phi_0}{Rc_0}. \quad (11)$$

Hence, the total active force density on the droplet along the  $x$  direction is positive in the contractile case ( $\zeta < 0$ ), which suggests that the droplet will be pushed in the positive  $x$  direction, as in our simulations (this conclusion can also be drawn from inspection of the pattern of active force distribution, Suppl. Fig. 3).

### 3.2.2 Homeotropic anchoring: extensile gel

Fig. 5 shows the case in which the active polar liquid crystal is extensile (for  $\zeta = 0.00001$ ); again with normal anchoring. The polarisation profile is virtually unchanged if compared to the contractile case; according to our analytical calculation reported above, one would thus expect the active forces to change sign leading to motion in the opposite direction. Simulations confirm this expectation: the droplet now moves with the defect at the front, rather than the rear (Suppl. Movie 3). At the same time, the force distributions in Figs. 4 and 5 are not related by a simple sign change. This is due in part to the

fact that an extensile fluid responds more to bend than to splay deformations (indeed in 1D it is only unstable to bend<sup>1</sup>). On the other hand, presumably as a result of the droplet colliding as it moves forward with the region of large deformation located at the defect core, the stability of the linear regime in an extensile environment is much diminished. Chaotic motion starts to occur already for  $\zeta = 0.00005$ , which is why a much smaller value is used in Fig. 5. This means however that the flow scale is much smaller in Fig. 5 than in Fig. 4, and indeed small enough to be partly masked by so-called ‘spurious currents’<sup>43</sup>. These are small but finite velocity values that arise when using lattice Boltzmann simulations, even in the quiescent state, due to the finite precision of the numerics. Therefore our results for the steady motility of an emulsion droplet with homeotropic anchoring in an extensile polar gel should be viewed as qualitative, not quantitative, in character.

### 3.2.3 Tangential anchoring

A significantly different dynamics is observed when tangential anchoring is imposed on the droplet surface. For simplicity, we focus here mainly on extensile gels, which leads to more interesting physics in this case. (We briefly comment below on the contractile version.) We note that this tangential anchoring may be more easily achieved than normal anchoring in experiments with extensile microtubule bundles such as those in Refs.<sup>30,31</sup>, as, due to their high stiffness (or persistence lengths) such bundles would presumably tend to follow the surface of a spherical inclusion.

Because tangential anchoring leads to a symmetric polarisation profile around the droplet (Fig. 2), we would expect any droplet motion to require symmetry breaking, and hence be associated with a non-zero activity threshold. In line with this expectation, we find that for small activity the droplet fails to move (Fig. 6). Interestingly, though, for the activity values in Fig. 6 for which the speed is zero, the droplet is not quite quiescent. Indeed, the values of  $\zeta$  in Fig. 6 are already large enough for spontaneous flow<sup>15–18</sup> to set up within the bulk of the extensile fluid (the threshold above which this occurs decreases with system size  $L$  as  $L^{-2}$ , hence it would be zero in the limit of an infinite system). The associated active flow shears the droplet, and continuously rotates it (Fig. 7). The direction of this rotation is persistent within a simulation, but varies according to the initial condition from one run to another, consistent with a spontaneous symmetry breaking mechanism. Note that the different geometry of the simulation box in Fig. 7 and Fig. 8 is chosen in anticipation of the direction of motion, which is perpendicular to the far field polarisation, rather than parallel to it as in Fig. 4 and in Fig. 5.

Fig. 6 shows also that for large enough  $\zeta$  the droplet begins to translate, in this case drifting downwards along the negative  $y$  direction (again the direction of motion is selected by spon-

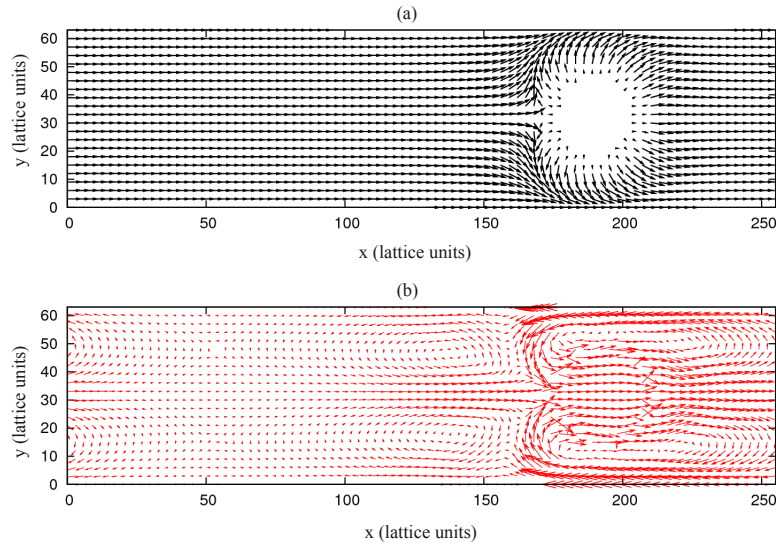


**Fig. 4** Polarisation field outside an isotropic droplet with homeotropic anchoring on its surface is reported in a) for the contractile case, with  $\zeta = -0.0001$  (corresponding to a contractile stress of 10 Pa according to the mapping in Appendix 1) and  $\kappa = 0.02$  (2 nN). A defect is still visible on the left, close to the surface of the droplet. The corresponding velocity field profile is in b). The flow pushes the droplet forward along the positive  $x$ -direction and four stretched vortices are generated by the contractile stress.

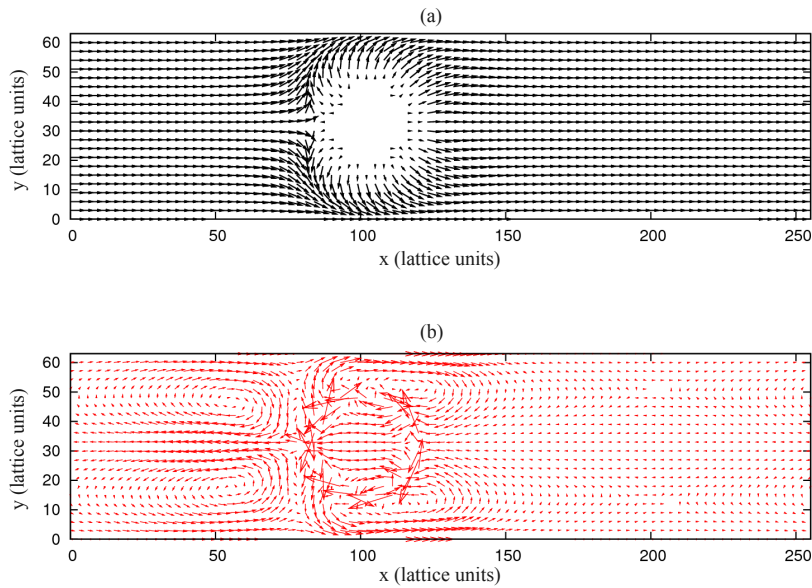


**Fig. 5** Polarisation field outside an isotropic droplet with homeotropic anchoring on its surface is reported in a) for the extensile case, with  $\zeta = 0.00001$  (corresponding to an extensile stress of 1 Pa according to the mapping in Appendix 1) and  $\kappa = 0.02$  (2 nN). As for the contractile case, a defect is located on the left of the droplet, close to its surface. The corresponding velocity field profile is in b). Now the flow pushes the droplet backward, along the negative  $x$ -direction and towards the defect. As the flow is much smaller (compare activity values in Fig. 5 and Fig. 4), spurious currents due to (well known<sup>43</sup>) numerical artifacts in the lattice Boltzmann scheme show up; the overall pattern of the flow field is still visible.

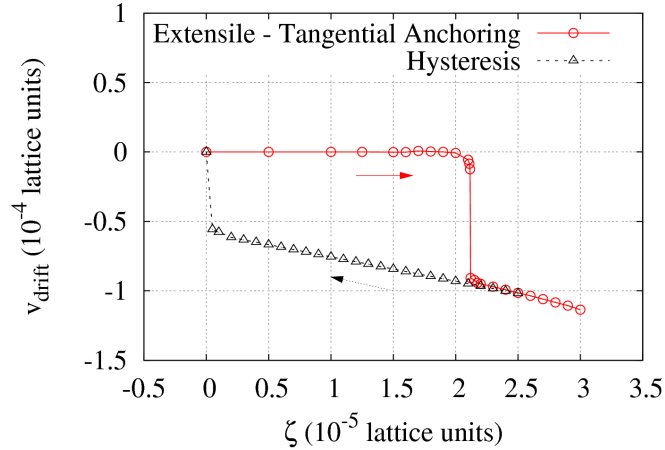


**Fig. 6** Steady state drift velocity as a function of the activity for an extensile system with tangential anchoring on the droplet's surface. Two different regimes, one in which the droplet is not moving (is at rest or rotates) and another one in which is moving, can be clearly distinguished before and after  $\zeta = \zeta_c \simeq 0.000021$  (or 2.1 Pa, see Appendix 1), respectively. Note the strong hysteresis observed on raising and then lowering activity.

taneous symmetry breaking). This is shown in Suppl. Movie 4 and Fig. 8, where it can be seen that the droplet now also stops rotating. Consistent with the change of symmetry, we find a sharp nonequilibrium transition between rotating and translationally motile states of the droplet at around  $\zeta_c \simeq 0.000021$ . Indeed we observed that there is strong hysteresis associated with this transition (see Fig. 6) which strongly corroborates its discontinuous character. The motility of the droplet in Fig. 8 is caused by the bend distortions close to the droplet surface, which lead to extensile active flows within the gel. In the motile state, as expected of a moving droplet, the deformations are asymmetric. As was seen for the contractile droplet with normal anchoring (Fig. 4), there are balancing currents, now at the sides of the droplet, and due to opposing bend deformation deeper in the active fluid.

Finally, we briefly comment on the case of emulsion droplets in *contractile* gels with tangential anchoring. Here again, motion does not occur for small  $\zeta$  as it requires spontaneous symmetry breaking, as for the case of the extensile/tangential gels just analysed. Furthermore, one would expect splay, rather than bend, deformations to cause the motion in a contractile medium, so that movement should occur along the far field polarisation rather than perpendicularly to it. However, we find that in the region where the droplet moves (for  $\zeta \leq -0.001$  in our simulations), the active flow in the contractile case is always unsteady, which leads to nonuniform droplet motion (Suppl. Movie 5).

### 3.2.4 Confined systems

As previously anticipated the threshold for the onset of spontaneous flow in an active fluid is known to scale as the inverse square of the system size, hence in a truly infinite system the passive phase would always be unstable. However, real systems have a finite size, and are often bounded by solid walls, and this can stabilise the passive phase for low activity<sup>‡</sup>. We therefore anticipate wall-bounded samples to behave very similarly, at least qualitatively, to the periodic systems considered thus far. To check that this is really the case, we also performed simulations in which a Newtonian droplet is confined between flat walls. For simplicity we have focused on the case in which the host is a contractile polar gel and homeotropic anchoring is imposed on the surface of the droplet. Furthermore, on both walls the polarisation is fixed parallel to the boundary, the concentration of active material has neutral wetting and the fluid velocity is zero (no-slip conditions). As in the corresponding case with periodic boundary conditions (see Fig. 4), the droplet is initially equilibrated in a passive gel and the activity is switched on afterwards. Fig. 9 shows that, as expected, the presence of boundaries does not affect significantly the physics of the droplet. In particular the droplet becomes motile and moves to the right, along the positive  $x$ -axis with the topological defect at its rear (as in Fig. 4). The fluid flow is now almost completely along the direction of motion. Increasing the activity  $\zeta$ , the system exhibits a turbulent-like behavior,

<sup>‡</sup> We also note that the periodic boundary simulations presented before can be replicated in the lab by using arrays or lattices of droplets rather than a single droplet.

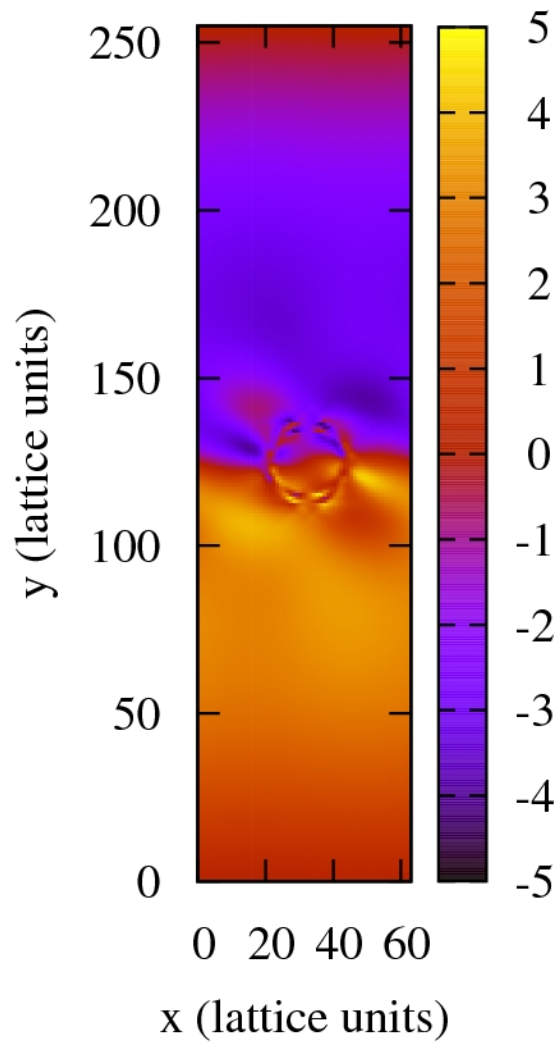


**Fig. 7** Velocity field profile for an isotropic droplet with tangential anchoring on its surface with  $\zeta = 0.00001 < \zeta_c$  ( $\zeta = 1$  Pa, see Appendix 1) and  $\kappa = 0.02$  (2 nN). The droplet rotates in anticlockwise direction due to a shear-like velocity field set up due to activity.

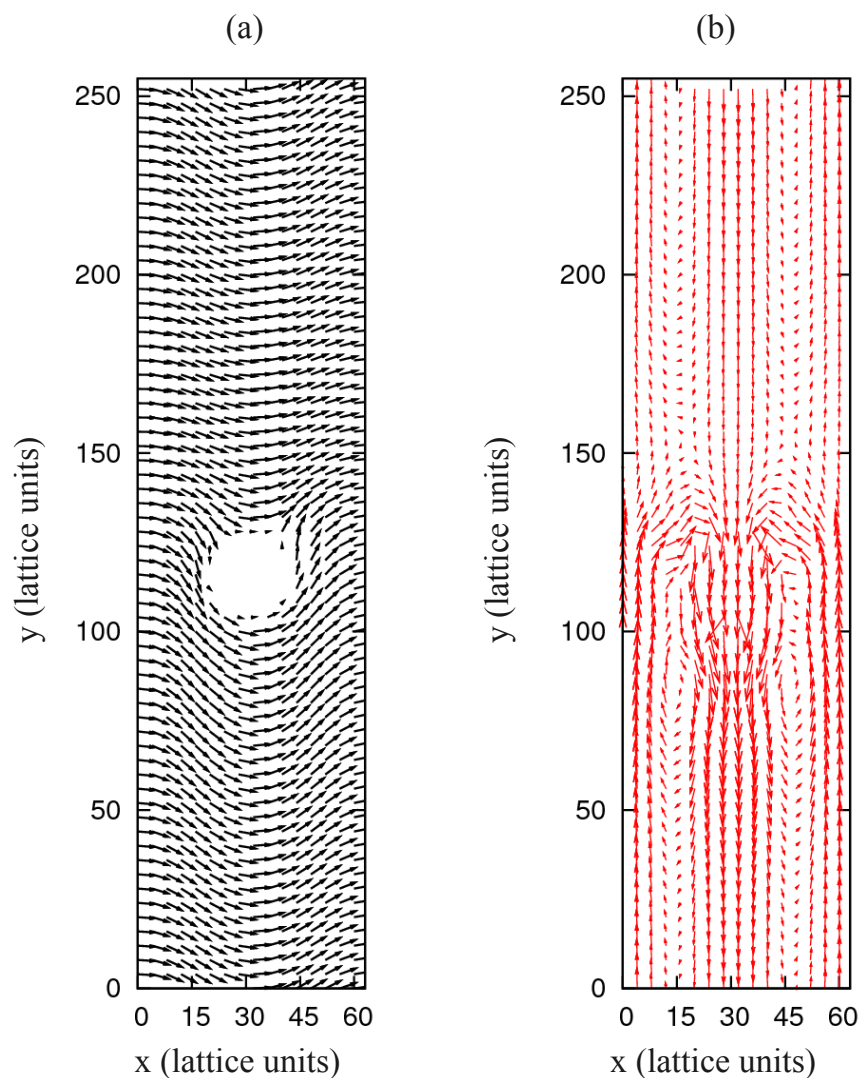


**Fig. 8** Polarisation field outside an isotropic droplet with tangential anchoring on its surface is reported in a) for the extensile case, with  $\zeta = 0.0001$  (10 Pa, see Appendix 1) and  $\kappa = 0.02$  (2 nN). Splay-bend distortions can be seen throughout the system, slightly more pronounced close to the droplet's surface. The corresponding velocity field profile is in b). The droplet is now moving along the negative  $y$ -direction. To avoid interactions with the periodic images along the main flow directions our simulation box now has size  $L_x = 64$  and  $L_y = 256$ .

again as expected from previous work<sup>18,20,22</sup> (data not shown). All this suggests that the phenomenology we described would be qualitatively similar with wall-bound systems (we hope to report on more detailed and quantitative effects of confinement elsewhere).

## 4 Conclusions

In conclusion, we studied here by computer simulations the dynamics of a passive droplet embedded in a polar active gel, either contractile (a simple model for actomyosin) or extensile (a simple model for a fluid of microtubule bundles and kinesin). We found that activity renders the physics of this composite material highly nontrivial.

First, we considered normal anchoring of the polarisation of the active gel at the droplet surface. Here the anchoring leads to an asymmetric dipolar polarisation field in equilibrium in the absence of activity, where a hyperbolic hedgehog appears at one side of the droplet. In the presence of any contractile activity (even infinitesimal), these polarisation patterns lead to an unbalanced force distribution, in which activity in the exterior gel phase is transduced by splay deformations and propels the droplet along an axis containing the defect and the droplet centre, with the defect at the rear. We identified a regime where the speed of the droplet increases with the activity linearly whereas for larger activity the motion becomes unsteady (and apparently chaotic). Extensile activity in the gel leads once more to motility at all activity levels with no threshold; however here the active flow pushes the droplet towards the defect rather than away from it, and this extra interaction leads to a significantly narrower linear regime.

Second, we studied the case of tangential anchoring of the polarisation at the droplet boundary. This boundary condition might possibly be more readily realised experimentally, as outlined in Section 3.2.3. Our computer simulations show that this case leads to different physics, and to an interesting nonequilibrium transition between a droplet which rotates due to the spontaneous active flow in the host, and a steadily moving droplet. In these cases, activity in the surrounding gel is transduced by bend deformations into either rotational motion (with a threshold that vanishes at large system sizes) or translational motility (with a threshold that remains finite). The latter transition occurs via symmetry breaking, and shares some similarities with the self-motile active droplets in an isotropic fluid studied in Ref.<sup>11</sup>. In contrast to the latter case, this transition appears discontinuous, and is associated with a large hysteresis loop, in which a finite propulsion speed can be sustained at a very small activity level by decreasing this from an initially larger value.

## 5 Acknowledgements

This work was funded in part by EPSRC grant no. EP/J007404. MEC holds a Royal Society Research Professorship.

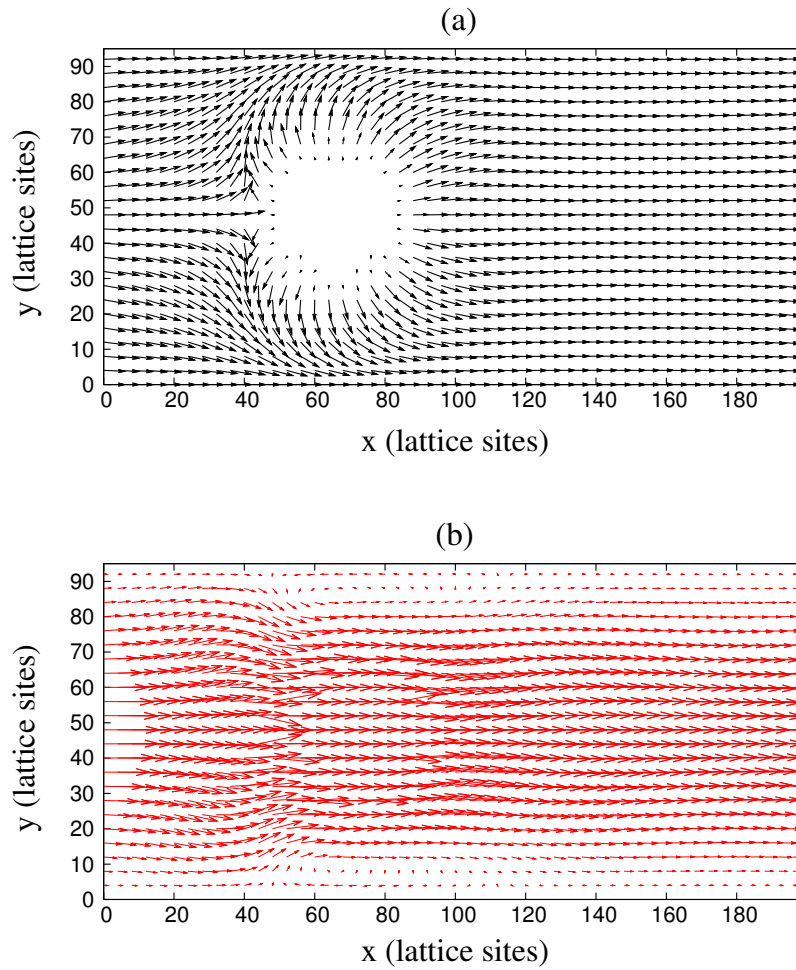
## 6 Appendix 1

Here we review the mapping between parameters used in our simulation and physical units. For concreteness, we consider the case of actomyosin (which is a contractile active gel). A correspondence between simulation and physical units in this context can be established by choosing length-scale, time-scale and force-scale to be:  $L = 1\mu\text{m}$ ,  $\tau = 10\text{ms}$  and  $F = 100\text{nN}$ , respectively<sup>11,32</sup>. All quantities are then determined through this correspondence, and their value in physical units is listed in Table I; for instance a contractile stress  $\zeta = 0.001$  in simulation units corresponds to  $\zeta = 100\text{ Pa}$ . This is a reasonable value for actomyosin<sup>44</sup>, as an individual myosin motor exerts a force of around 1 pN, and there can be  $\sim 100$  motors within a  $1\mu\text{m}^3$  actomyosin volume for a  $1\mu\text{M}$  motor concentration, suggesting that that typical stress values are (for that concentration) of order  $\sim 100\text{ pN}/\mu\text{m}^2 = 100\text{ Pa}$ . We should also note that, as in previous lattice Boltzmann simulations<sup>11,32</sup>, we chose the fluid mass density to be much larger than the actual mass density of a real solvent (water)<sup>45</sup>. This works so long as the Reynolds number (i.e. inertial effects) remains small and speeds up the computations by several orders of magnitude. In our case the Reynolds number is below  $\sim 0.02$  in all cases, which is small enough to be in the laminar regime.

Finally, the extensile microtubule-kinesin gels of Ref.<sup>30,31</sup> are also composite materials made up by cytoskeletal filaments and molecular motors, the mapping to real units for those systems would therefore be related to that of actomyosin, although slightly different values may be more appropriate in that case (for instance the force exerted by a single kinesin motor is  $\sim 5\text{ pN}$ , and microtubules are often longer than actin fibres<sup>46</sup>).

## References

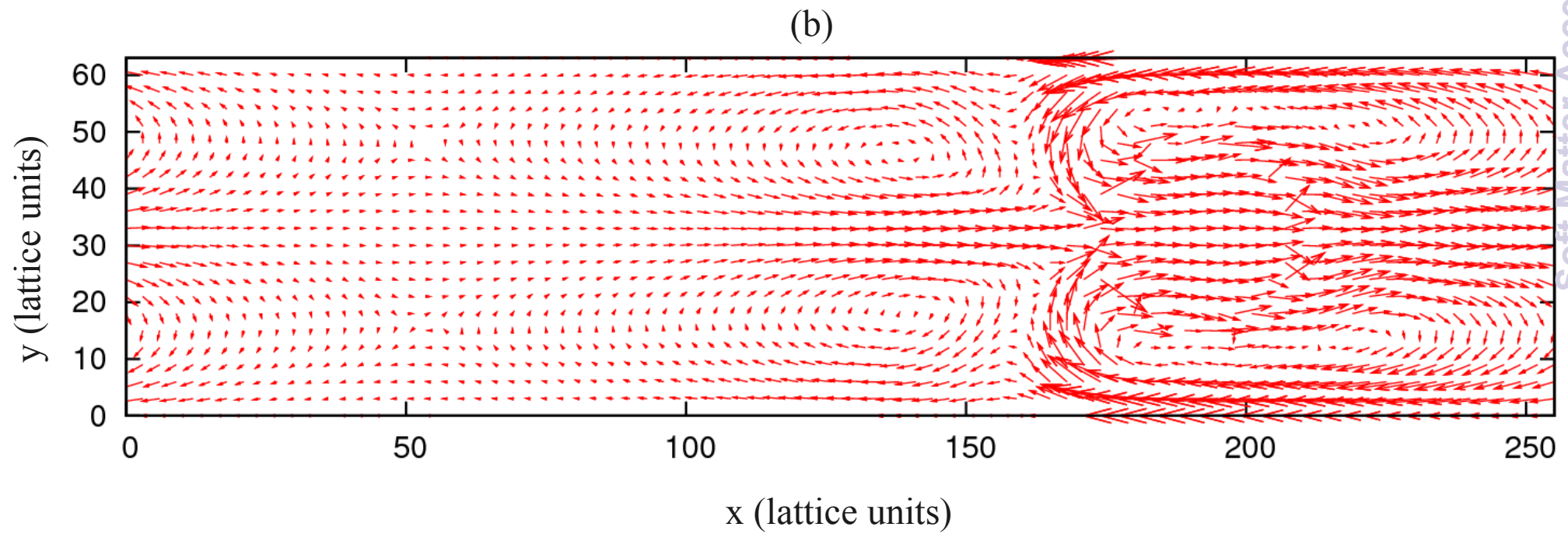
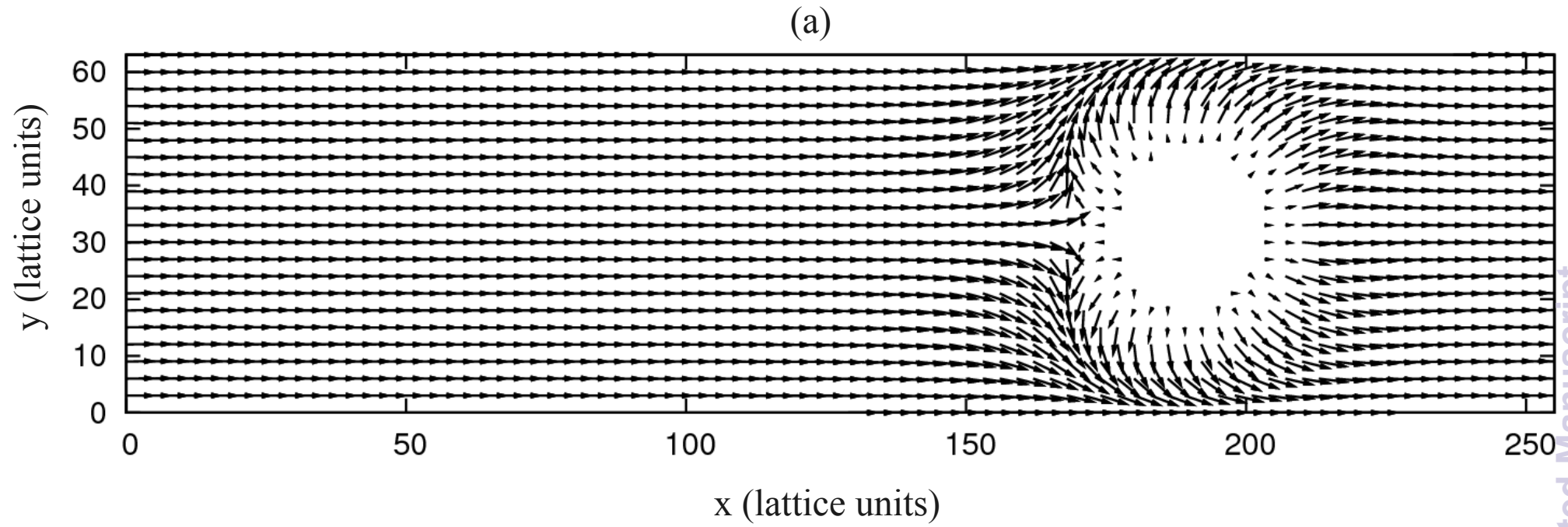
- 1 M. C. Marchetti, J. F. Joanny, S. Ramaswamy, T. B. Liverpool, J. Prost, M. Rao, and R. A. Simha, *Rev. Mod. Phys.* **85**, 1143 (2013).
- 2 S. Ramaswamy, *Annual Review of Condensed Matter Physics* **1**, 323 (2010).
- 3 I. Llopis and I. Pagonabarraga, *Europhys. Lett.* **75**, 999 (2006)
- 4 J. Stenhammar, A. Tiribocchi, R. J. Allen, D. Marenduzzo, M. E. Cates, *Phys. Rev. Lett.* **111**, 145702 (2013).



**Fig. 9** Polarisation field outside an isotropic droplet in a contractile host and confined between flat walls (a). There is normal anchoring on the droplet surface, and there is tangential anchoring at the walls. Parameters are as in Section 2, except  $\zeta = -0.00005$  (corresponding to a contractile stress of 5 Pa, see Appendix 1),  $k\phi_{cr} = 0.14$  (14 nN),  $\kappa = 0.05$  (5 nN). The simulation box has size  $L_x = 200$  and  $L_y = 96$  (200 and 96  $\mu\text{m}$  respectively). The corresponding velocity field profile is in b).

Model variables and parameters (actomyosin)	Simulation units	Physical units
Effective shear viscosity, $\eta$	1	1 kPa · s
Effective elastic constant, $\kappa$	0.01 – 0.02	1 – 2 nN
Shape factor, $\xi$	1.1	dimensionless
Effective diffusion constant, $D = Ma$	0.004	$0.4 \mu\text{m}^2/\text{s}$
Rotational viscosity, $\Gamma$	1	1 kPa · s
Activity, $\zeta$	0 – 0.001	(0 – 0.1) kPa

- 5 J. Bialke, T. Speck, H. Lowen, *Phys. Rev. Lett.* **108**, 168301 (2012).
- 6 T. Ohta, T. Ohkuma, *Phys. Rev. Lett.* **102**, 154101 (2009).
- 7 M. Tarama, T. Ohta, *Phys. Rev. E* **87**, 062912 (2013).
- 8 S. Yabunaka, T. Ohta, N. Yoshinaga, *J. Chem. Phys.* **136**, 074904 (2012).
- 9 N. Yoshinaga, *Phys. Rev. E* **89**, 012913 (2014).
- 10 S. Thutupalli, R. Seemann, S. Herminghaus, *New Jour. of Phys.* **13**, 073021 (2011).
- 11 E. Tjhung, D. Marenduzzo, M. E. Cates, *Proc. Natl. Acad. Sci. USA* **109**, 12381-12386 (2012).
- 12 C. A. Whitfield, D. Marenduzzo, R. Voituriez, R. J. Hawkins, *Eur. Phys. J. E* **37** 8 (2014).
- 13 L. Giomi, A. De Simone, *Phys. Rev. Lett.* **112**, 147802 (2014).
- 14 K. Kruse, J.-F. Joanny, F. Julicher, J. Prost, K. Sekimoto, *Phys. Rev. Lett.* **92**, 078101 (2004).
- 15 R. Voituriez, J.-F. Joanny, J. Prost, *Europhys. Lett.* **70**, 404 (2005).
- 16 R. Voituriez, J.-F. Joanny, and J. Prost, *Phys. Rev. Lett.* **96**, 028102 (2005).
- 17 D. Marenduzzo, E. Orlandini, and J. M. Yeomans, *Phys. Rev. Lett.* **98**, 118102 (2007).
- 18 D. Marenduzzo, E. Orlandini, M. E. Cates, and J. M. Yeomans, *Phys. Rev. E* **76**, 031921 (2007).
- 19 L. Giomi, M. C. Marchetti, and T. B. Liverpool, *Phys. Rev. Lett.* **101**, 198101 (2008).
- 20 L. Giomi, L. Mahadevan, B. Chakraborty, and M. F. Hagan, *Phys. Rev. Lett.* **106**, 218101 (2011).
- 21 M. E. Cates, S. M. Fielding, D. Marenduzzo, E. Orlandini, and J. M. Yeomans, *Phys. Rev. Lett.* **101**, 068102 (2008).
- 22 S. M. Fielding, D. Marenduzzo, and M. E. Cates. *Phys. Rev. E* **83**, 041910 (2011).
- 23 L. Giomi, T. B. Liverpool, and M. C. Marchetti, *Phys. Rev. E* **81**, 051908 (2010).
- 24 G. Foffano, J. S. Lintuvuori, K. Stratford, M. E. Cates, and D. Marenduzzo, *Phys. Rev. Lett.* **109**, 028103 (2012).
- 25 G. Foffano, J. S. Lintuvuori, A. N. Morozov, K. Stratford, M. E. Cates, D. Marenduzzo, *Euro. Phys. Journ. E* **35**, 10 (2012).
- 26 M.S. Silva, M. Depken, B. Stuhmann, M. Korsten, F.C. MacKintosh, and G.H. Koenderink, *Proc. Natl. Acad. Sci. U.S.A.* **108**, 9408 (2011).
- 27 P. M. Bendix *et al.*, *Biophys. J.* **94**, 3126-3136 (2008).
- 28 A. Sokolov, I. S. Aranson, J. O. Kessler, and R. E. Goldstein, *Phys. Rev. Lett.* **98**, 158301 (2007).
- 29 L. H. Cisneros, R. Cortez, C. Dombrowski, R. E. Goldstein, J. O. Kessler, *Exp. Fluids* **43**, 737 (2007).
- 30 T. Sanchez *et al.*, *Nature* **491**, 431 (2012).
- 31 T. Sanchez, Z. Dogic, *Meth. in Enzymol.* **254**, 205 (2013).
- 32 E. Tjhung, A. Tiribocchi, D. Marenduzzo, M. E. Cates, submitted for publication.
- 33 Y. Hatwalne, S. Ramaswamy, M. Rao, A. R. Simha, *Phys. Rev. Lett.* **92**, 118101 (2007).
- 34 P. G. de Gennes and J. Prost, *The Physics of Liquid Crystals, 2nd Ed.*, Clarendon Press, Oxford (1993).
- 35 M. E. Cates, O. Henrich, D. Marenduzzo, K. Stratford, *Soft Matter* **5**, 3791 (2009).
- 36 E. Tjhung, M. E. Cates, D. Marenduzzo, *Soft Matter* **7**, 7453 (2011).
- 37 H. Stark, *Phys. Rep.* **351**, 387 (2001).
- 38 G. Foffano, J. Lintuvuori, A. Tiribocchi, D. Marenduzzo, *Liq. Cryst. Rev.*, in press (2014).
- 39 G. P. Alexander, B. Gin-ge Chen, E. A. Matsumoto, and R. D. Kamien, *Rev. Mod. Phys.* **84**, 497 (2012).
- 40 T. C. Lubensky, D. Petey, N. Currier, and H. Stark, *Phys. Rev. E* **57**, 610 (1998).
- 41 P. Poulin, H. Stark, T. Lubensky, and D. Weitz, *Science* **275**, 1770 (1997).
- 42 P. Poulin, D. A. Weitz, *Phys. Rev. E* **57**, 1 (1998).
- 43 K. Connington, T. Lee, *Journ. Mech. Sci. & Tech.* **26**, 3857 (2012); C. M. Pooley and K. Furtado, *Phys. Rev. E* **77**, 046702 (2008).
- 44 B. Rubinstein, M. F. Fournier, K. Jacobson, A. B. Verkhovsky, A. Mogilner, *Biophys. J.* **97**, 1853 (2009).
- 45 M. E. Cates, K. Stratford, R. Adhikari, P. Stansell, J.-C. Desplat, I. Pagonabarraga, A. J. Wagner, *J. Phys. Cond. Mat.* **16**, S3903 (2004).
- 46 B. Alberts *et al.*, *Molecular Biology of the Cell*, Garland Science, New York (2002).



We study a Newtonian droplet in a polar active gel: we find that activity makes the droplet move.